Inorg. Chem. **2008**, *47*, 4088−4094

Growth Mechanism and Optical Properties of Aligned Hexagonal ZnO Nanoprisms Synthesized by Noncatalytic Thermal Evaporation

Ahmad Umar,† B. Karunagaran, S. H. Kim, E.-K. Suh, and Y. B. Hahn*

School of Semiconductor and Chemical Engineering, BK21 Centre for Future Energy Materials and Devices, Semiconductor Physics Research Centre, Chonbuk National University, Jeonju 561-756, South Korea

Received September 28, 2007

Vertically aligned perfectly hexagonal-shaped ZnO nanoprisms have been grown on a Si(100) substrate via a noncatalytic thermal evaporation process by using metallic zinc powder in the presence of oxygen gas. The as-grown nanoprisms consist of ultra smooth Zn-terminated (0001) facets bounded with the $\{01\bar{1}0\}$ surfaces. The as-synthesized products are single-crystalline with the wurtzite hexagonal phase and grown along the [0001] direction, as confirmed from the detailed structural investigations. The presence of a sharp and strong nonpolar optical phonon high-E_2 mode at 437 cm^{-1} in the Raman scattering spectrum further confirms good crystallinity and wurtzite hexagonal phase for the as-grown products. The as-grown nanoprisms exhibit a strong near-band-edge emission with a very weak deep-level emission in the room-temperature and low-temperature photoluminescence measurements, confirming good optical properties for the deposited products. Moreover, systematic time-dependent experiments were also performed to determine the growth process of the grown vertically aligned nanoprisms.

I. Introduction

Wurtzite hexagonal structured ZnO is one of the most important II−VI group semiconductor possessing a direct and wide band gap of 3.37 eV, large exciton binding energy of 60 meV, much higher than other semiconductor materials such as GaN (25 meV) and ZnSe (22 meV), and high optical gain of 300 cm^{-1} (100 cm^{-1} for GaN) at room-temperature.[1,2] Because of its wide band gap at room-temperature, it is suitable for the fabrication of efficient short-wavelength optoelectronic devices such as light-emitting diodes (LEDs) and laser diodes (LDs).[3] The high-exciton binding energy of ZnO, larger than the thermal energy at room-temperature (26 meV), make it a good candidate for the fabrication of room-temperature UV LDs.[4] Because of the noncentrosymmetric structure of ZnO, it exhibits a piezoelectric nature which is a cardinal property for the fabrication of electromechanical coupled sensors, actuators, and transducers.[5] By exploring piezoelectric properties of ZnO nanostructures, recently Wang and co-workers have made nanogenerators which were able to convert the mechanical energy into electric energy.[6] These kinds of nanogenerator devices have great potential for harvesting energy from the environment and for self-powering nanodevices. [6] In addition to this, the biocompatible and biosafe nature of ZnO makes them an important material for biomedical applications.[7] Therefore, because of the extraordinary and versatile properties and wide applications of ZnO, it has been described as one of the most important materials after carbon nanotubes in terms of functionality and applications.[6] Heretofore, a variety of ZnO nanostructures have been prepared using various fabrication techniques and reported in the literature.[8–17] Among the

* To whom correspondence should be addressed. E-mail: ybhahn@chonbuk.ac.kr. Fax: +82-63-270-2306.
† E-mail: ahmadumar@chonbuk.ac.kr.

(1) Huang, M. H.; Mao, S.; Feick, H.; Yan, H. Q.; Wu, Y.; Kind, H.; Weber, E.; Russo, R.; Yang, P. D. *Science* **2001**, *292*, 5523.
(2) Choopun, S.; Vispute, R. D.; Noch, W.; Balsamo, A.; Sharma, R. P.; Venkatesan, T.; Iliadis, A.; Look, D. C. *Appl. Phys. Lett.* **1999**, *75*, 3947.
(3) Service, R. F. *Science* **1997**, *276*, 895.
(4) Ryu, Y. R.; Zhu, S.; Budai, J. D.; Chandrasekhar, H. R.; Miceli, P. F.; White, H. W. *J. Appl. Phys.* **2000**, *88*, 201.
(5) Kuoni, A.; Holzherr, R.; Boillat, M.; de Rooij, N. F. *J. Micromech. Microeng.* **2003**, *13*, S103.
(6) (a) Wang, Z. L.; Song, J. H. *Science* **2006**, *312*, 242. (b) Song, J. H.; Zhou, J.; Wang, Z. L. *Nano Lett.* **2006**, *6*, 1656. (c) Gao, P. G.; Song, J. H.; Liu, J.; Wang, Z. L. *Adv. Mater.* **2007**, *19*, 67. (d) Wang, Z. L. *MRS Bull.* **2007**, *32*, 109. (e) Wang, Z. L. *Adv. Mater.* **2007**, *19*, 889. (f) Wang, X. D.; Song, J. H.; Liu, J.; Wang, Z. L. *Science* **2007**, *316*, 102. (g) Wang, X. D.; Liu, J.; Song, J. H.; Wang, Z. L. *Nano Lett.* 2007, in press. (h) Wang, Z. L. *Materials Today* **2007**, *10*, 20–28.
(7) Zhou, J.; Xu, N. S.; Wang, Z. L. *Adv. Mater.* **2006**, *18*, 2432–2435.
(8) Umar, A.; Lee, S.; Lee, Y. S.; Nahm, K. S.; Hahn, Y. B. *J. Cryst. Growth* **2005**, *277*, 479.

10.1021/ic701929p CCC: $40.75
Published on Web 04/09/2008

various kinds of ZnO nanostructures, the 1D (one-dimensional) nanostructures such as nanorods and nanoprisms have a special place due to their great prospects in fundamental physical science and nanotechnology applications and their significant potentials for nanooptoelectronics.[1–17] Previously, Lin et al. demonstrated the synthesis and optical characterization of ZnO nanorods, grown by a thermal evaporation process by using mixtures of high-purity ZnO and carbon powder at 980 °C on Au-coated sapphire substrates.[18] Ng et al. reported the synthesis of 1D ZnO nanostructures on a Au-coated m-sapphire substrate by using a mixture of ZnO and graphite powders at 1000 °C in 2 h via a catalyst-assisted heteroepitaxial carbothermal reduction approach.[19] Zhang et al. synthesized the ZnO nano- and microrods and arrays on the cylindrically shaped substrate by thermal evaporation using metallic zinc powder at the temperature ranges between 650 and 850 °C in 60–120 min.[20] Recently, Liu et al. successfully grew the ZnO hexagonal nanoprisms onto a Au-coated silicon substrate at 910 °C using the ZnO and activated carbon in 120 min.[21] Zhao et al. also demonstrated the synthesis of ZnO nanorods on a ZnO/Si substrate by a thermal evaporation process by using ZnO and graphite powders at 950 °C.[22a] Recently, Khan et al. also synthesized ZnO nanorods on Si substrates by using zinc powder at the temperature ranges between 600– 700 °C.[22b] In all the results mentioned above, the obtained products were grown at higher temperature with the assistance of catalyst/additives or buffer layer. Moreover, all the results shown above exhibited UV emission, but broad green emissions are also seen in the room-temperature photoluminescence (PL) spectra, which are related to the structural defects and impurities of the corresponding structures. Nevertheless, it is important to have an enhanced ultraviolet-emission in the PL spectra of the synthesized products to utilize them for the fabrication of efficient UV-nanooptoelectronic devices in near future.

In this paper, we are reporting the structural and optical properties of the vertically aligned highly perfect hexagonal-shaped ZnO nanoprisms composed of ultra smooth Zn-terminated (0001) facets bounded with the $\{01\bar{1}0\}$ surfaces. These nanoprisms were grown via a simple thermal evaporation process by using metallic zinc powder in the presence of oxygen on Si(100) substrates at 570 °C without the use of any metal catalyst/additives or buffer layers. The detailed PL properties, observed at room- and low-temperature, of as-grown nanoprisms reveals a strong ultraviolet-emission which confirmed that the grown products have excellent optical properties. In addition to this, several time dependent experiments were performed to investigate the detailed growth mechanism of the as-grown nanoprisms on silicon substrates.

II. Experimental Procedures

Aligned perfectly hexagonal-shaped ZnO nanoprisms were synthesized in a horizontal quartz tube furnace. Commercially available high-purity metallic zinc (99.999%) and oxygen (99.999%) were used as source materials for zinc and oxygen, respectively. Si(100) substrates were used to deposit the products. Prior to loading the substrates into the furnace, they were treated for 10 min with the buffer solution to remove the native oxide layer, washed with deionized water, acetone, and methanol, and finally dried with inert gas (N_2). In a typical reaction process, ~2 g of metallic zinc powder was put into a small quartz boat and placed at the center of the quartz tube furnace. The silicon substrate was placed 2 cm away from the source material. Before the evaporation, the reaction chamber was purged with high purity argon gas for 30 min. After this arrangement, the furnace was heated up to 650 °C with the heating rate of 25 °C/min under the continuous flow of nitrogen gas (30 sccm; standard cubic centimeters per minute). After attaining the desired temperature (650 °C), a mixture of high-purity nitrogen and oxygen gases were introduced into the reactor furnace with flow rates of 50 and 20 sccm, respectively. The furnace temperature was kept constant at 650 °C during whole reaction process. The substrate temperature was measured with a moveable thermo-couple and found to be 570 °C. The reaction lasted 75 min. After terminating the reaction, the furnace was allowed to cool rapidly at room temperature. During the reaction, the zinc vapor was heated, vaporized, and transported along the carrier gas, and a gray colored product was deposited onto the substrates which were characterized in detail in terms of their structural and optical properties.

Structural characterizations of the as-grown products were done by using field emission scanning electron microscopy (FESEM), transmission electron microscopy (TEM), and high resolution TEM (HRTEM) equipped with the selected area electron diffraction (SAED) and X-ray diffraction (XRD) patterns measured with Cu Kα radiation. Raman scattering spectra were measured at room temperature with the Ar^+ laser line ($\lambda = 513.4$ nm) as excitation source. The PL measurements excited by the 325 nm line from the He−Cd laser were done at room temperature and low temperatures in the range of 11–300 K.

III. Results and Discussion

A. Detailed Structural Properties of As-Synthesized Hexagonal-Shaped Vertically Aligned ZnO Nanoprisms. Figure 1 shows the FESEM images of the as-grown products which clearly reveal that the deposited products are regular hexagonal-shaped nanoprisms, vertically aligned, and grown in high-density over the whole substrate surface. Figure 1 a,b shows the top-view FESEM images of the as-grown ZnO nanoprisms. As can be seen from the high-magnification image, all the nanoprisms are formed with the six crystallographic planes where all the planes are connected to each other with internal angles of ~60°, representing the exact

(9) Umar, A.; Kim, S. H.; Lee, Y. S.; Nahm, K. S.; Hahn, Y. B. *J. Cryst. Growth* **2005**, *282*, 131.
(10) Umar, A.; Hahn, Y. B. *Appl. Phys. Lett.* **2006**, *88*, 173120.
(11) Zhang, B. P.; Binh, N. T.; Wakatsuki, K.; Segawa, Y.; Yamada, Y.; Usami, N.; Koinuma, H. *Appl. Phys. Lett.* **2004**, *84*, 4098.
(12) Hughes, W. L.; Wang, Z. L. *Appl. Phys. Lett.* **2003**, *82*, 2886.
(13) Umar, A.; Lee, S.; Im, Y. H.; Hahn, Y. B. *Nanotechnology* **2005**, *16*, 2462.
(14) Gao, P. X.; Wang, Z. L. *J. Appl. Phys.* **2005**, *97*, 044304.
(15) Kong, X. Y.; Wang, Z. L. *Appl. Phys. Lett.* **2004**, *84*, 975.
(16) Hughes, W. L.; Wang, Z. L. *J. Am. Chem. Soc.* **2004**, *126*, 6703.
(17) Umar, A.; Hahn, Y. B. *Nanotechnology* **2006**, *17*, 2174.
(18) Lin, J. M.; Lin, H. S.; Cheng, C. L.; Chen, Y. F. *Nanotechnology* **2006**, *17*, 4391.
(19) Ng, H. T.; Chen, B.; Li, J.; Han, J.; Meyyappan, M.; Wu, J.; Li, S. X.; Haller, E. E. *Appl. Phys. Lett.* **2003**, *82*, 2023.
(20) Zhang, Y.; Wang, L.; Liu, X.; Yan, Y.; Chen, C.; Zhu, J. *J. Phys. Chem. B* **2005**, *109*, 13091.
(21) Liu, D. F.; Xiang, Y. J.; Zhang, Z. X.; Wang, J. X.; Gao, Y.; Song, L.; Liu, L. F.; Dou, X. Y.; Zhao, X. W.; Luo, S. D.; Wang, C. Y.; Zhou, W. Y.; Wang, G.; Xie, S. S. *Nanotechnology* **2005**, *16*, 2665.

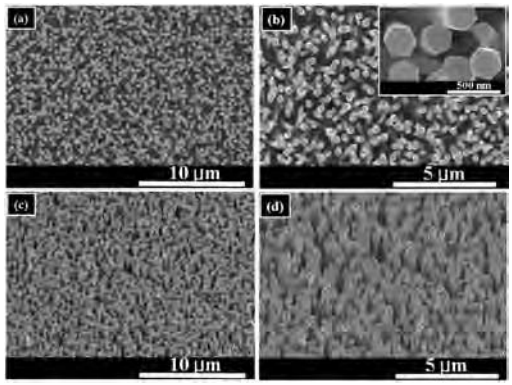

Figure 1. (a) Low and (b) high magnification top view FESEM images and (c, d) 45° tilted FESEM images of the hexagonal-shaped vertically aligned ZnO nanoprisms grown on Si substrates.

nature of the hexagonal crystal system (Figure 1b). The as-grown nanoprisms exhibit a uniform size distribution along the axis, sharp edges, and flat top and side surfaces. Moreover, the as-grown nanoprisms contain the (0001) top facets enclosed with six equivalent $\{01\bar{1}0\}$ crystal planes. Therefore, the apparent hexagonal surfaces with facets confirmed the epitaxial growth and single crystalline nature with the *c*-axis as the preferred orientation of the as-grown products. The typical diameters of the as-grown nanoprisms are in the range of 200 ± 50 nm while the lengths lie in the range of 5 ± 1 μm. Figure 1 c,d shows the 45° tilted view of the ZnO nanoprisms which further confirm that the formed nanoprisms are perpendicular to the substrate surface and are grown in a very high density over the whole substrate.

The crystal phase, crystallinity, and compositions of the as-deposited aligned ZnO nanoprisms were observed by their XRD pattern and energy dispersive spectroscopy (EDS), respectively, and shown in Figure 2. Figure 2a shows the typical XRD pattern for the ZnO nanoprisms grown onto a Si(100) substrate. All the observed peaks in the pattern are well matched with the reported values of wurtzite hexagonal phase pure bulk ZnO (Joint Committee on Powder Diffraction Standards, JCPDS Card No. 75-1526). A strongest peak at 69.1° has been found in the pattern which is related to the silicon substrate and assigned Si(004). In addition to this, a peak at 34.2° attributed as ZnO(0002) is the dominant among all other ZnO peaks in the pattern, indicating that the as-grown nanoprisms are single crystalline and grown preferentially along the [0001] direction. Moreover, except for ZnO, no peaks from other impurities, such as unreacted zinc, are detected from the pattern, which confirmed that the as-grown nanoprisms are purely wurtzite hexagonal phase ZnO. Figure 2b shows the typical EDS spectrum of the as-synthesized ZnO nanoprisms, which reveals that the as-synthesized products are composed of zinc and oxygen only. No other peak for other impurities were found in the spectrum; however, the appearance of the silicon peak is due to the substrate. The detailed structural characterizations of the as-synthesized product were done by TEM and HRTEM.

Figure 3a shows the low-magnification TEM image of the as-grown ZnO nanoprisms and exhibits full consistency with the FESEM observations in terms of their morphology and

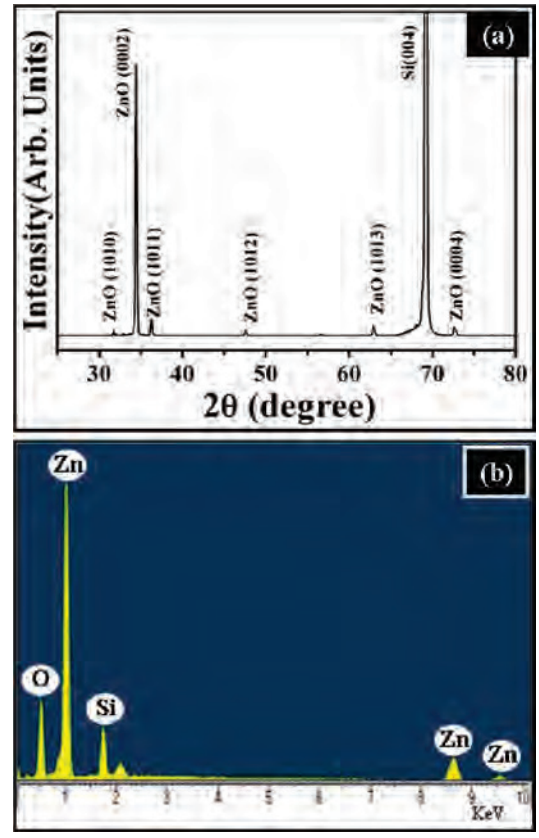

Figure 2. (a) XRD pattern and (b) EDS spectrum of the hexagonal-shaped vertically aligned ZnO nanoprisms grown on Si substrates.

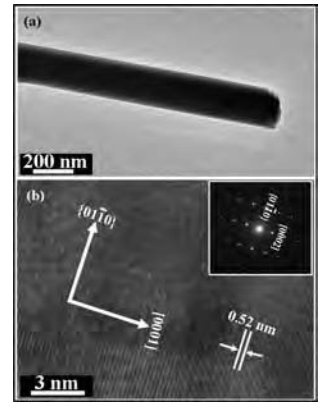

Figure 3. (a) Low magnification TEM image of an individual ZnO nanoprism. (b) High magnification TEM (HRTEM) image of the ZnO nanoprism exhibiting single crystallinity, grown along the [0001] direction with the 0.52 nm distance between two lattice fringes. The corresponding SAED pattern (inset of (b)) is consistent with the HRTEM result.

dimensionality. The as-grown nanoprisms are defect free and possess smooth and clean surfaces throughout their lengths. The HRTEM image of the corresponding nanoprisms displayed in Figure 3a is shown in Figure 3b; it clearly exhibits the distances between two parallel lattice fringes, which is about ~0.52 nm and corresponds to the (0001) planes of the wurtzite hexagonal phase ZnO, confirming that the grown nanoprisms are single crystalline with the wurtzite hexagonal phase and grown preferentially along the (0001) direction. Furthermore, no dislocation or stacking faults were observed from the synthesized products. The corresponding SAED pattern is well matched and exhibits consistency with

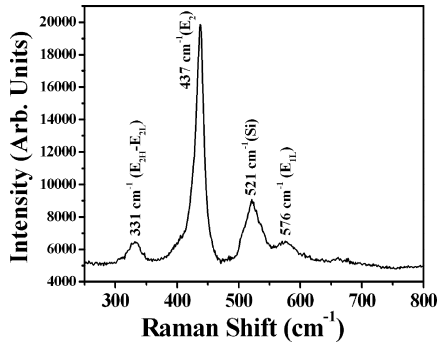

Figure 4. Typical Raman scattering spectrum of the as-grown hexagonal-shaped vertically aligned ZnO nanoprisms grown on Si substrates.

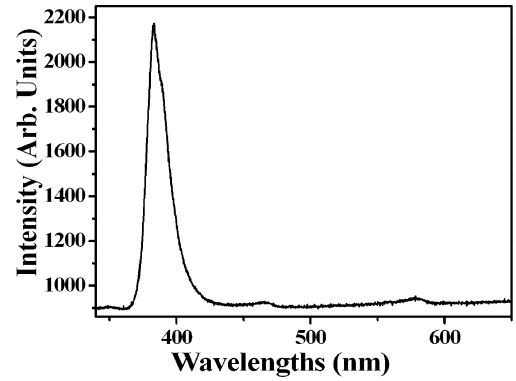

Figure 5. Typical room-temperature PL spectrum of the as-grown hexagonal-shaped vertically aligned ZnO nanoprisms grown on Si substrates.

the HRTEM observation. This further affirms the single crystallinity with the *c*-axis preferred orientation for the synthesized ZnO nanoprisms (Figure 3b inset).

B. Detailed Optical Properties of As-Synthesized Hexagonal-Shaped Vertically Aligned ZnO Nanoprisms. The optical properties of the as-synthesized hexagonal-shaped aligned ZnO nanoprisms were examined by using Raman scattering and PL measurements. With a wurtzite hexagonal phase, ZnO belongs to the space group C^4_{6v} ($P6_3mc$). Group theory predicts that the zone centered optical phonon-symmetry is $\Gamma = A_1 + 2B_1 + E_1 + 2E_2$,[23,24] where A_1, E_1, and E_2 modes are Raman active while the B_1 modes are silent. Additionally, the A_1 and E_1 are infrared active and therefore split into longitudinal and transverse optical (LO and TO) components while E_2 is Raman-active only.[24] Figure 4 exhibits the typical Raman scattering spectrum for the as-grown aligned hexagonal-shaped ZnO nanoprisms. According to the previously reported results, the strongest band among all other observed peaks in the spectrum, obtained at 437 cm^{-1}, can be assigned as a nonpolar optical-phonon high E_2 mode, which appeared because of the wurtzite hexagonal phase of ZnO.[23,24] Moreover, a band at 331 cm^{-1} has been observed which is assigned as $E_{2H} - E_{2L}$ (multiphonon process) and can be found only when the ZnO is single crystal.[25] A much suppressed peak at 576 cm^{-1} attributed as an E_{1L} mode (corresponds to E_1 symmetry with LO mode) has also been seen. Generally, it is believed that an E_{1L} mode is related to the formation of defects in ZnO.[17,24] Additionally, the presence of a peak at 521 cm^{-1} is due to the silicon substrate. Therefore, the presence of a strong peak of a nonpolar optical phonon high E_2 mode and a suppressed E_{1L} mode confirmed that the as-synthesized ZnO nanoprisms have good crystal quality with the wurtzite hexagonal phase.

Figure 5 shows the typical room-temperature PL spectrum of the as-grown hexagonal-shaped aligned ZnO nanoprisms. The room-temperature PL spectrum of ZnO typically consists of a UV emission and possibly one or more visible emissions. The as-grown ZnO nanoprisms exhibited a sharp, strong, dominant, and high intensity peak at 382 nm in the UV region while two much suppressed and weak bands at 470 and 581 nm in the blue-green regions were also observed in the spectrum. The UV emission is also called a near-band-edge (NBE) emission and originated because of the recombination of free-excitons through an exciton–exciton collision process.[26] The green emission is also known to be a deep level emission (DPE) which is caused by the impurities and structural defects in the crystal such as oxygen vacancies, zinc interstitials, and so forth. The mechanism of green emission has been proposed and reported by Vanheusden et al., namely, that the origination of the green emission is due to the recombination of the electrons in singly occupied oxygen vacancies in ZnO and the emission results due to the recombination of a photogenerated hole with an electron occupying the oxygen vacancies.[27] About the strong peak of the UV emission, it is also reported that the improvement in the crystal-quality such as low structural defects, oxygen vacancies, zinc interstitials and the decrease in the impurities may cause the appearance of a sharp and strong UV emission and a suppressed and weak green emission.[28] As in our case, the UV emission is dominant over the blue-green emission; hence, it confirmed that the as-grown ZnO nanoprisms have good crystal quality with far fewer structural defects and possess excellent optical properties. The room-temperature PL spectrum is also consistent with the TEM and Raman observations.

The detailed optical properties of the grown ZnO nanorods were done by low-temperature PL spectra. Figure 6 and 7 show the low-temperature PL spectra of the as-grown hexagonal-shaped aligned ZnO nanoprisms measured using a He−Cd laser line of 325 nm as the excitation source with the excitation power of 30 mW. The low-temperature PL spectrum of the as-grown ZnO nanoprisms taken at 11 K is shown in Figure 6 which shows the presence of strong UV emission in the band-edge region with several distinct peaks. To determine the accurate peak positions, experimental data

(22) (a) Zhao, D.; Andreazza, C.; Andreazza, P.; Ma, J.; Liu, Y.; Shen, D. *Chem. Phys. Lett.* **2005**, *408*, 335. (b) Khan, A.; Jadwisienczakb, W. M.; Lozykowskib, H. J.; Kordesch, M. E. *Physica E* **2007**, *39*, 258.
(23) Arguelo, C. A.; Rousseau, D. L.; Porto, S. P. S. *Phys. Rev.* **1969**, *181*, 1351.
(24) Calleja, J. M.; Cardona, M. *Phys. Rev. B* **1977**, *16*, 3753.
(25) Yang, Y. H.; Wang, C. X.; Wang, B.; Li, Z. Y.; Chen, J.; Chen, D. H.; Xu, N. S.; Yang, G. W.; Xu, J. B. *Appl. Phys. Lett.* **2005**, *87*, 183109.
(26) Kong, Y. C.; Yu, D. P.; Zhang, B.; Fang, W.; Feng, S. Q. *Appl. Phys. Lett.* **2001**, *78*, 407.
(27) Vanheusden, K.; Seager, C. H.; Warren, W. L.; Tallant, D. R.; Voigt, J. A. *J. Appl. Phys.* **1996**, *79*, 7983.
(28) Bagnall, D. M.; Chen, Y. F.; Zhu, Z.; Yao, T.; Koyama, S.; Shen, M. Y.; Goto, T. *Appl. Phys. Lett.* **1998**, *73*, 1038.

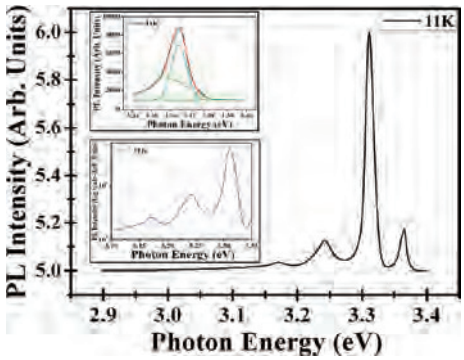

Figure 6. Typical PL spectrum measured at 11 K of the as-grown hexagonal-shaped vertically aligned ZnO nanoprisms grown on Si substrates. Upper inset is the high-magnification PL spectrum measure at 11 K and lower inset is the semilogarithmic plot at 11 K of the as-grown nanoprisms.

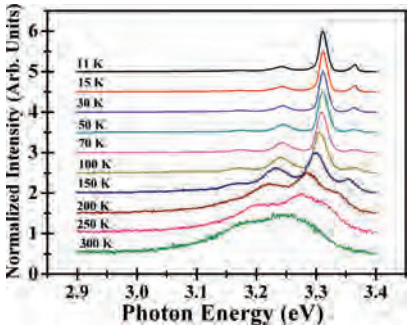

Figure 7. Temperature-dependent PL spectra of the vertically aligned hexagonal-shaped ZnO nanoprisms measured in the range of 11−300 K.

were fitted using a Gaussian line shape function. Actually, the band-edge PL in bulk ZnO can be divided into seven regions: free excitons (FX, 3.3769 eV < E < 3.49 eV), excitons-bound to ionized donors (D^+X, 3.36499 eV < E < 3.3769 eV), excitons-bound to neutral-donors (D°X, 3.36088 eV < E < 3.36499 eV), excitons-bound to neutral-acceptors (A°X, 3.35409 eV < E < 3.36088 eV), exciton complexes with deep centers (3.3333 eV < E < 3.35407 eV), two-electron transitions (3.3155 eV < E < 3.3333 eV), and phonon replica region (<3.3155 eV).[29–32]

A zoom-in view of the spectroscopic region from 3.34 to 3.4 eV is shown in the upper inset of Figure 6 which shows the existence of free excitons (FX) at 3.37688 eV and of a neutral donor-bound exciton (D°X) at 3.36432 eV for the as-grown nanoprisms. In typical ZnO films or bulk crystals, the FX band is not clearly observed at low temperatures because of the localization of excitons by impurities, especially due to donors. At high temperatures, usually around 50–70 K, the FX band is predominant because of the ionization of impurities that are used to bind excitons at low temperature.[33–37] The observation of the FX band in the emission spectrum even at a very low temperature of 11 K for as-grown nanoprisms suggests that the as-grown products possess good optical properties with very low levels of impurities. According to the conventions mentioned above, the strong and dominant peak in Figure 6 is ascribed to the first order TO phonon replica of the free-exciton recombination with a maximum at 3.3155. The reason for the assignment is that the energy spacing between this peak and the free-exciton peak is close to the transverse phonon energy (~61 meV).[34,38] The evidence for this assignment is further supported by the temperature dependence of the peaks as discussed below. The strong emission intensity of the TO phonon peaks suggests a strong coupling of the TO phonon and the free exciton. Also, the 3.3155 eV emission band is commonly observed in the high-quality ZnO epitaxial films, nanocrystalline films, and nanorods, which is due to the donor–acceptor pair (DAP) recombination.[39–41]

The semilogarithmic plot shown in the lower inset of Figure 6 reveals the existence of an additional PL peak energetically below the bound-exciton complexes with a main peak at 3.24174 eV. This peak is attributed to the free-excitonic emission including the TO and the first order LO phonons (71.9 meV) because the energy difference between this line and the FX is close to the sum of the energies of the TO and LO phonons.

The temperature dependence of the PL spectra for selected temperatures between 11 and 300 K is shown in Figure 7. These spectra clearly illustrate that the exciton-emission is shifted to lower energy (red-shift) with increasing temperature. As can be seen in Figure 7, the intensities of the bound excitons (D°X) and FX were found to decrease with increase in temperature. The emission band DAP also showed strong emission at elevated temperatures. The FX and D°X emissions were found to quench as the temperature was increased. But comparatively, the FX peak intensity was found to improve with the increase in temperature relative to the D°X peak intensity. The FX peak intensity almost exceeds the D°X peak intensity around 70 K, and above 70 K, we believe that the D°X peak almost disappears, which results thus in only the DAP peak being identified from the spectra. Also it is clear from the spectrum that the bound-excitons emission could not be resolved and it may be because of the thermal dissociation at high- temperatures. As the temperature increases further, this peak shifts to the lower energy side and dramatically decreases in intensity while DAP emission becomes more prominent relative to the FX emission. With further increase of temperature, only the DAP emission is

(29) Tomzig, E.; Helbig, R. *J. Lumin.* **1976**, *14*, 403.
(30) Umar, A.; Karunagaran, B.; Suh, E.-K.; Hahn, Y. B. *Nanotechnology* **2006**, *17*, 4072.
(31) Klingshirn, C. F. *Semiconductor Optics*; Springer: Berlin, 1995.
(32) Studenikin, S. A.; Cocivera, M.; Kellner, W.; Pascher, H. *J. Lumin.* **2000**, *91*, 223.
(33) Jie, J.; Wang, G.; Chen, Y.; Han, X.; Wang, Q.; Xu, B.; Hou, J. G. *Appl. Phys. Lett.* **2005**, *86*, 031909.
(34) Zhang, Y.; Lin, B.; Sun, X.; Fui, Z. *Appl. Phys. Lett.* **2005**, *86*, 131910.
(35) Mikami, M.; Eto, T.; Wang, J. F.; Masa, Y.; Isshiki, M. *J. Cryst. Growth* **2005**, *276*, 389.
(36) Reynolds, D. C.; Look, D. C.; Jogai, C. B.; Litton, W.; Collins, T. C.; Harsch, W.; Antwell, G. *Phys. Rev. B* **1998**, *57*, 12151.
(37) Ogata, K.; Kawanishi, T.; Maejima, K.; Sakurai, K.; Fujita, Sz.; Fujita, Sg. *Jpn. J. Appl. Phys., Part 2* **2001**, *40*, L657.
(38) Decremps, F.; Porres, J. P.; Saita, A. M.; Cheervin, J. C.; Polian, A. *Phys. Rev. B* **2002**, *65*, 092101.
(39) Bagnall, D. M.; Chen, Y. F.; Shen, M. Y.; Zhu, Z.; Goto, T.; Yao, T. *J. Cryst. Growth* **1998**, *84/185*, 605.
(40) Zhang, X. T.; Liu, Y. C.; Zhi, Z. Z.; Zhang, J. Y.; Lu, Y. M.; Shen, D. Z.; Xu, W.; Zhong, G. Z.; Fan, X. W.; Kong, X. G. *J. Phys. D: Appl. Phys.* **2001**, *34*, 3430.
(41) Zhang, B. P.; Binh, N. T.; Segawa, Y.; Wakatsuki, K.; Usami, N. *Appl. Phys. Lett.* **2003**, *83*, 1635.

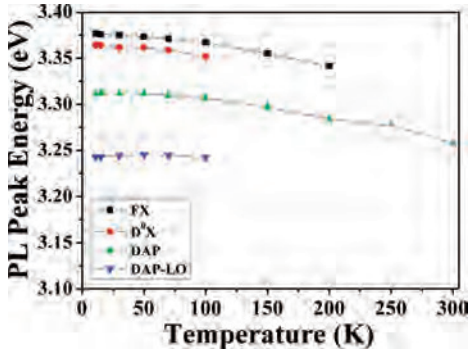

Figure 8. PL peak energies as a function of temperature.

dominantly observed. This feature clearly reveals the DAP transitions without any band-to-impurity transitions.

The temperature dependence of the NBE PL peak positions is depicted in Figure 8. The FX, D°X, and DAP emissions systematically shift to lower energy (red-shift) with increasing temperature. The D°X emissions are found to thermally quench around 100 K, consistent with what has been reported for bulk ZnO. For semiconductors with a direct band gap, if the exciton binding energy is independent of the temperature, the band edge exciton emission peak shifts to lower energy (red-shift) as the temperature of the ZnO nanorod is increased with the peak energy following the empirical relation,

$$E(T) = E(0) - \frac{\alpha T^2}{T + \beta} \quad (1)$$

where $E(0)$ is the emission energy at 0 K. The parameters α and β are fitting parameters to be determined by curve fitting to the experimental data. The above Varshini empirical formula successfully describes the temperature dependence of the FX peak positions. Given that the binding energy of the FX is nearly independent of the temperature, $E(0)$, α, and β are 3.377 eV, 1.5×10^{-4} eV K^{-1}, and 2800 K, respectively. The results of the best fit are represented by dotted lines through the data points in Figure 8. The value of $E(0)$ for the free exciton emission is estimated to be 3.377 eV, and it agrees well with the reported one for bulk ZnO. The value of β is also found to be in reasonable agreement with the recently reported value within the error.[30,42]

C. Growth Mechanism of the As-Synthesized Hexagonal-Shaped Vertically Aligned ZnO Nanoprisms. A metal catalyst was neither used nor detected in the products; hence, we attribute that the growth process for the formation of aligned hexagonal-shaped ZnO nanoprisms in our experiments is the vapor−solid (VS) process[10,17] rather than the conventionally and commonly used vapor–liquid–solid (VLS) process[43] in which nanosized metal particles have been used which act as a catalyst for the growth of the nanostructures. The main characteristic of the VLS mechanism is the presence of metal nanoparticles on the tips of the grown nanostructures. To clearly understand the growth process of the as-grown aligned hexagonal-shaped ZnO nanoprisms, time dependent experiments, by keeping other reaction parameters the same, were performed and are shown in

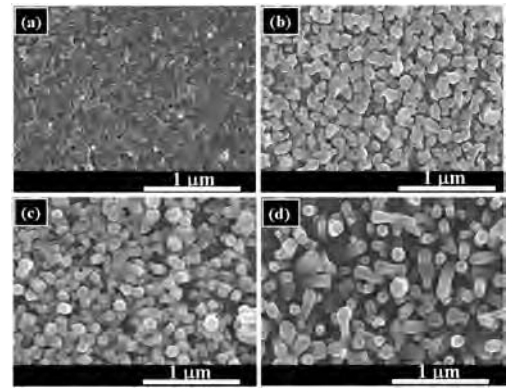

Figure 9. FESEM images of the schematic growth process for the formation of ZnO nanorods onto the Si(100) substrate: (a) after reaching the temperature of the furnace up to ~650 °C, and after (b) 7 min, (c) 15 min, and (d) 22 min growth durations.

Figure 9. By the clear examination of the various growth stages at different growth times, one can provide insight into the growth mechanism of the aligned hexagonal-shape ZnO nanoprisms. (Figure 9a−d) shows the various growth stages at different growth times, that is, after the temperature of the furnace reached up to ~650 °C under nitrogen flow, the growth at 7, 15, and 22 min, respectively. As can be seen from the micrographs, the growth of the nanorods can be divided into two parts: nucleation and growth. After placing the substrate and source material into the quartz tube, when the temperature of the furnace was increased to 650 °C with the flow of high-purity nitrogen gas, the zinc-vapors were generated (melting point of Zn = 419.5 °C) from the source material, metallic zinc powder. The generated zinc vapors were transported by the nitrogen carrier gas and covered the whole substrate surface in the form of zinc film (Figure 9a). By introducing the oxygen gas, the deposited zinc film reacted with the oxygen and started to nucleate which leads to the formation of ZnO nuclei onto the substrate surface in the early 7 min of the reactions (Figure 9b). This will be the nucleation process. After this nucleation process, the incoming species (zinc vapors and oxygen) were reacted in the gas phase via a simple chemical reaction $Zn(g) + O_2(g) \rightarrow ZnO(g)$. The gaseous ZnO is deposited onto the previously formed ZnO nuclei as the reaction proceeds (Figure 9c). With time, the deposition over the ZnO nuclei increases which leads the formation of small ZnO nanoprisms in 22 min (Figure 9d). By increasing more the reaction time, these small hexagonal nanoprisms directed the growth of the long-length perfectly hexagonal-shaped aligned ZnO nanoprisms (Figure 1). In a crystal point of view, the shapes of the crystals depend upon the relative growth rates of the various crystal planes. Therefore, the high-index crystal plane with small interplanar spacing grows faster than the low index-planes and thus are not seen in the final shape of the crystals.[44,45] As the ideal growth rates of the wurtzite hexagonal ZnO crystals in different directions are found in the order of [0001] > $[01\bar{1}\bar{1}]$ > $[01\bar{1}0]$ > $[01\bar{1}1]$ > $[000\bar{1}]$ under hydrothermal conditions,[46,47] it has tendency to form faceted single

(42) Chen, S.; Liu, Y.; Shao, C.; Mu, R.; Lu, Y.; Zhang, J.; Shen, D.; Fan, X. *Adv. Mater.* **2005**, *17*, 586.
(43) Gao, P. X.; Wang, Z. L. *J. Phys. Chem. B* **2004**, *108*, 7534.
(44) Donnay, J. D. H.; Harker, D. *Am. Mineral.* **1937**, *22*, 446.
(45) Mariano, A. N.; Hanneman, R. E. *J. Appl. Phys.* **1963**, *34*, 384.

crystalline hexagonal-shaped particles which contain the ±{0001} crystal planes at their top and bottom and enclosed by the six equivalent {01$\bar{1}$0} crystal facets.[46,47] As can be seen in Figure 9b,c when the oxygen reacts with the zinc, they formed the hexagonal ZnO nanoparticles which possess the {0001} and {01$\bar{1}$0} crystal phases and act as seeds for the further growth of the final nanoprisms. Additionally, with increasing the reaction time, adsorption over the {0001} surfaces increases more as compared to the {01$\bar{1}$0} facets; hence, growth of the nanoparticles dominated in the *c*-axis and finally 1D anisotropic hexagonal ZnO nanoprisms were obtained (Figure 9d). Moreover, the wurtzite hexagonal crystal structured ZnO is composed of O^{2-} and Zn^{2+} ions arranged in a tetrahedral manner and stacked alternatively along the *c*-axis direction. ZnO also has a polar nature and hence contains the positively charged Zn-(0001) surfaces, which are catalytically active, and the negatively charged O-(0001) surfaces, which are chemically inert.[10,43] Therefore, the growth velocity of the [0001] crystal planes are faster than other growth facets because of the presence of Zn-terminated (0001) surfaces which are catalytically active and contain the self-catalytic growth property. Interestingly, in our synthesized aligned hexagonal-shaped ZnO nanoprisms, it also exhibits smooth and clean Zn-terminated {0001} planes with the highly perfect hexagonal surface facets, bounded with the six-crystallographic {01$\bar{1}$0} planes and grown along the [0001] direction. Therefore, one can conclude that the morphologies of the as-grown nanoprisms are fully consistent with the ideal anisotropic growth behavior of ZnO crystals.

(46) Laudise, R. A.; Ballman, A. A. *J. Phys. Chem.* **1960**, *64*, 688.
(47) Laudise, R. A.; Kolb, E. D.; Caporaso, A. J. *J. Am. Ceram. Soc.* **1964**, *47*, 9.

IV. Conclusions

In summary, ultra smooth Zn-terminated (0001) facets bounded with the {01$\bar{1}$0} surfaces, vertically aligned perfectly hexagonal-shaped ZnO nanoprisms were grown on a silicon substrate by a noncatalytic thermal evaporation process. The extensive structural investigations using FESEM, HRTEM, SAED, and XRD revealed that the as-grown nanoprisms are single-crystalline possessing wurtzite hexagonal phase and are preferentially grown along the *c*-axis, in the [0001] direction. The Raman scattering and room-temperature PL spectrum substantiated that the synthesized ZnO nanoprisms are good in crystal quality with a wurtzite hexagonal phase and exhibit good optical properties. At low temperature PL spectra, it has been found that the Varshini expression can give adequate prediction of the free-exciton and bound-exciton peak positions at different temperatures. Finally, based on the time dependent experiments, a growth mechanism for the formation of aligned ZnO nanoprisms is discussed in detail. Therefore, because of their high-crystallinity and UV PL property, the as-grown ZnO nanoprisms can be useful for the fabrication of efficient opto-electronic devices in near future.

Acknowledgment. This work was supported in part by the Brain Korea 21 project in 2007 and the Korea Research Foundation Grant KRF-2005-005-J07502 (MOEHRD). The authors wish to thank Mr. T. S. Bae and J. C. Lim, KBSI, Jeonju branch, and Mr. Jong-Gyun Kang, Centre for University Research Facility (CURF) for taking good quality FESEM and TEM images, respectively.

IC701929P